Thermomechanical Analysis of Printed Circuit Heat Exchangers for Optimization of Supercritical CO_2-based Power Cycles in Concentrated Solar Power

Christopher J. Hyland[1], Josh M. Petry[1], Robert L. Lowe[1], Justin DelMar[2], Andrew J. Schrader[1]*

[1]Department of Mechanical & Aerospace Engineering, University of Dayton, Dayton, OH 45469-0238, USA
[2]Aerospace Systems Directorate, Air Force Research Laboratory, Wright-Patterson AFB, OH 45433, USA
*Corresponding author | email: aschrader1@udayton.edu

Abstract

Simulation, analysis, and optimization of sCO_2 Brayton power cycles was performed by leveraging advanced computational techniques, including machine learning and genetic algorithms, to address the multi-dimensional challenges of cycle and component design. Machine learning models were used as an intermediary in predicting specific cycle design criteria performance metrics from simulated data, enhancing system flexibility and computational efficiency. In parallel, multi-objective optimization was orchestrated through the NSGA-II algorithm, navigating the trade-offs between cycle efficiency and component mass. Heat exchanger sizing was based on a revisited stress analysis, where the implications of several common assumptions were explored. The optimization process yielded a multi-dimensional Pareto front of potential optimal solutions which showed system objective trade-offs through multi-criteria decision-making techniques.

1. Introduction

Supercritical carbon dioxide (sCO_2) power cycles have the potential to deliver higher thermal efficiencies while simultaneously providing increased flexibility in key design criteria such as footprint, component mass, source heat rates, cycle temperatures, and mass flow rates. However, the enhanced flexibility of these design criteria presents a significant challenge when considering the pace of innovation surrounding these cycles and their components. Previous literature in this space has showcased the potential of sCO_2 Brayton power cycles [1], investigated specific cycle components such as turbomachinery and heat exchangers [2], and optimized design criteria and cycle parameters for specific applications such as concentrated solar power (CSP), nuclear energy [3], non-renewable energy sources[4], and on-board power systems [5].

Printed circuit heat exchangers (PCHEs) coupled with sCO_2 represent current and future research areas in the field of thermal management and energy conversion. PCHEs offer significant advantages in terms of compactness, efficiency, and performance in high-pressure and high-temperature applications. PCHEs are characterized by their microchannel patterns etched or printed onto metal plates before being diffusion bonded together.

Machine learning and multi-objective optimization via genetic algorithms have become increasingly pivotal in the field sCO_2 power cycle optimization. These advanced computational techniques offer robust solutions to the complex, multi-dimensional problems inherent in the design and operation of sCO_2 power systems. Machine learning algorithms facilitate the prediction and generalization of system behaviors from vast datasets, enabling the efficient handling of uncertainties and variabilities in operational parameters and system applications. Concurrently, multi-objective optimization – particularly genetic algorithms like NSGA-II – provides a framework for addressing the trade-offs between conflicting objectives such as size, weight, performance, and cost constraints. These methods are inherently suited to the multi-criteria nature of power system optimization and are used to identify Pareto-optimal solutions which include a set of equally optimal solution candidates.

2. System Simulation and Optimization

Cycle and turbomachinery simulation processes are constructed using an in-house modular cycle simulation program in `Python`. In order to simulate a wide range of cycle and turbomachinery design criteria, most major specifications were generated using Latin Hypercube Sampling (LHS) methods across comprehensive ranges, including cycle maximum temperatures, coolant inlet temperatures, working fluid and coolant mass flow rates, turbine and compressor efficiencies, effectiveness of heat exchangers, high and low cycle pressures, and turbomachinery spindle speeds. Thermodynamic properties of the working fluid and coolant were referenced using the database `REFPROP` (v.10.0, NIST [6]), allowing for a more accurate evaluation of properties throughout the system.

2.1. Cycle Simulation

Four generalized cycle architectures were investigated to capture a wider range of design criteria: direct heating recuperated cycle (Fig. 1a), direct heating non-recuperated cycle (Fig. 1b), indirect heating recuperated cycle (Fig. 1c), and indirect heating non-recuperated cycle (Fig. 1d). These four cycles were chosen to capture behavior with both direct and indirect heating of the working fluid as well as additionally recuperated variations of these two generalized cycle configurations.

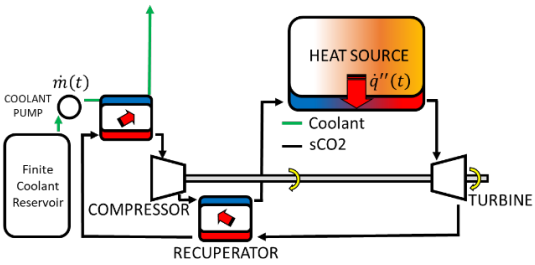

Figure 1a: Direct Heating - Recuperated Cycle

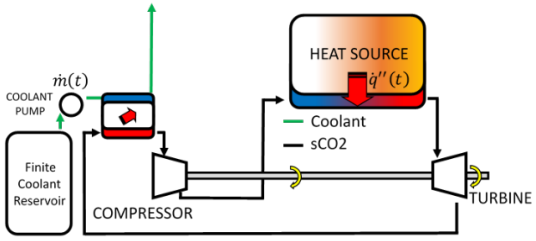

Figure 1b: Direct Heating - Non-Recuperated Cycle

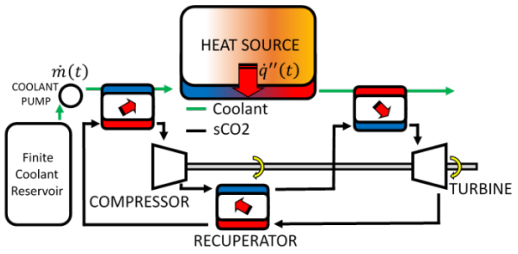

Figure 1c: Indirect Heating - Recuperated Cycle

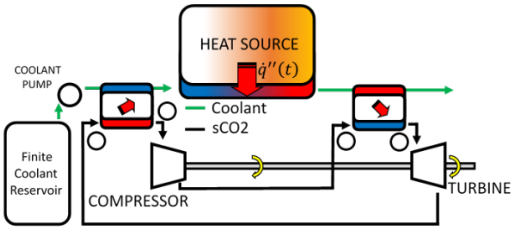

Figure 1d: Indirect Heating - Non-Recuperated Cycle

The simulation function of each of the cycle architectures was built in a similar structure utilizing a common set of subsystem functions for simulating the process and behavior of each cycle component, followed by an update of the system's thermodynamic properties at the given state point. This allowed for more efficient development of new cycle architecture simulation functions and the ability to improve or interchange individual components for each cycle architecture.

The cycle simulation output was multifaceted, providing a comprehensive analysis of the Brayton cycle. Key outputs included detailed thermodynamic properties at each stage of the cycle such as temperature, pressure, enthalpy, and entropy, while also providing performance indicators including net work output and thermal efficiency. Performance metrics for individual components, including efficiency ratios, work output or input, and heat transfer rates, are calculated and presented.

2.2. Machine Learning and Multi-Objective Optimization

Critical components of the optimization process were individual trained models that acted as intermediaries between the raw data from the simulated cycle architectures and turbomachinery, and the optimization procedures. These trained models increase the range and flexibility of the system while reducing the computational complexity needed to analyze a large number of design criteria.

This optimization procedure was designed for multi-objective optimization in the context of sCO_2 Brayton cycles, utilizing machine learning models and genetic algorithms. The program integrated `TensorFlow` [7] for neural network models, and `pymoo` [8] for multi-objective optimization.

A multi-objective optimization was performed using the NSGA-II algorithm, focusing on maximizing cycle efficiency and minimizing turbine and compressor mass. Pre-trained neural network models were utilized to predict performance metrics based on input parameters, with the optimization problem defined in the Problem class specifying variables, objectives, and bounds. The NSGA-II algorithm iteratively improved a solution population through selection, crossover, and mutation, based on the defined objectives. Upon completion, optimal solutions and objectives were extracted, denormalized using pre-loaded model parameters, and saved for further analysis. The objective points obtained from the NSGA-II algorithm culminate in a multi-dimensional Pareto front, representing the most favorable objective points derived from the set of optimal solutions. These objective Pareto fronts manifest in a space that corresponds to the dimensionality of the optimization objectives. Specifically, when the solutions are mapped into a three-dimensional space, they form a surface referred to as the Pareto front. This surface illustrates the trade-offs among the three objectives, demonstrating how each solution on the Pareto front offers a different balance of these objectives. Additionally, multi-criteria decision-making techniques, such as pseudo weights and high trade-off points, are applied to the optimization results, providing insights into the objective space and identifying solutions with specific characteristics.

3. Heat Exchanger Stress and Sizing Analysis

The mechanics of PCHEs and the implications of some common assumptions adopted from the literature were investigated in the model with the ultimate goal of improving PCHE sizing predictions for a variety of sCO_2 heat exchangers. Widely used geometric simplifications were employed to simplify PCHEs with semi-circular channels to be modeled as rectangular pressure vessels [9-12]. A schematic of the representative triple-slot pressure vessel, given in Fig. 2, was applied for the stress analysis and sizing of PCHEs in sCO_2 cycles. This adjustment allowed for direct application of the stress analysis in Ref. [14] to the revised triple slot pressure vessel model (Fig. 2). The amended model consists of three rectangular channels representative of those in a full-scale heat exchanger: an "interior" channel embedded between two stay plates (orange), and two "exterior" channels flanked by a stay plate (orange) and short-side plate (red). The channels are enclosed at top and bottom by the long-side plate (blue).

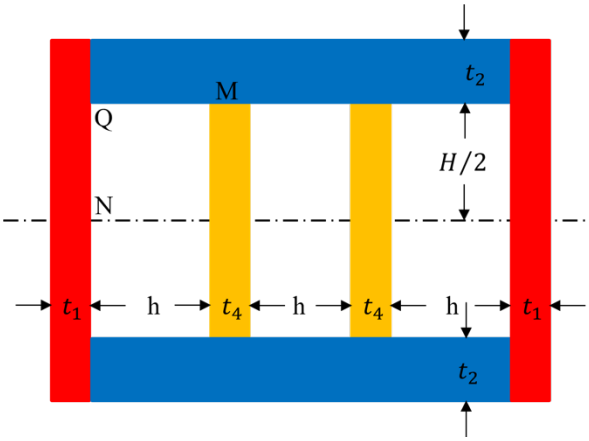

Figure 2: A schematic of the representative triple-slot pressure vessel, was applied for the stress analysis and sizing of PCHEs in sCO_2 cycles.

Reference [14] regards each of the key structural elements – short-side plate, long-side plate, and stay plate – as rectangular members capable of supporting both membrane and bending stresses. Importantly, in contrast to some previous investigations in the literature, investigations did not include a common *a priori* assumption that the moment of inertia ratio (K) approaches zero. Recent investigations often omit *c*, the distance from the neutral axis to extreme fiber, in

their analyses [9, 10, 12]. Following Ref. [10], the channel failure criterion is regarded as when the total stress (membrane plus bending) in a particular structural member exceeds 1.5 times the design stress; where the design stress is the product of allowable stress (obtained from Ref. [13]) and a joint factor of 0.7. Utilizing a MATLAB script with the stress equations from Ref [14] and the failure criteria from Refs. [9, 14], component thicknesses (i.e., t_1, t_2, and t_4 in Fig. 2) were calculated. Note that for the short-side members, stresses were calculated at the mid-span (N) and the corner (Q). Similarly, for the long-side members, stresses were calculated at the mid-span (M) and corner (Q). The most conservative (largest) thickness for each element (corresponding to the stress "hotspot" of the two queried locations) were selected as the modeled value.

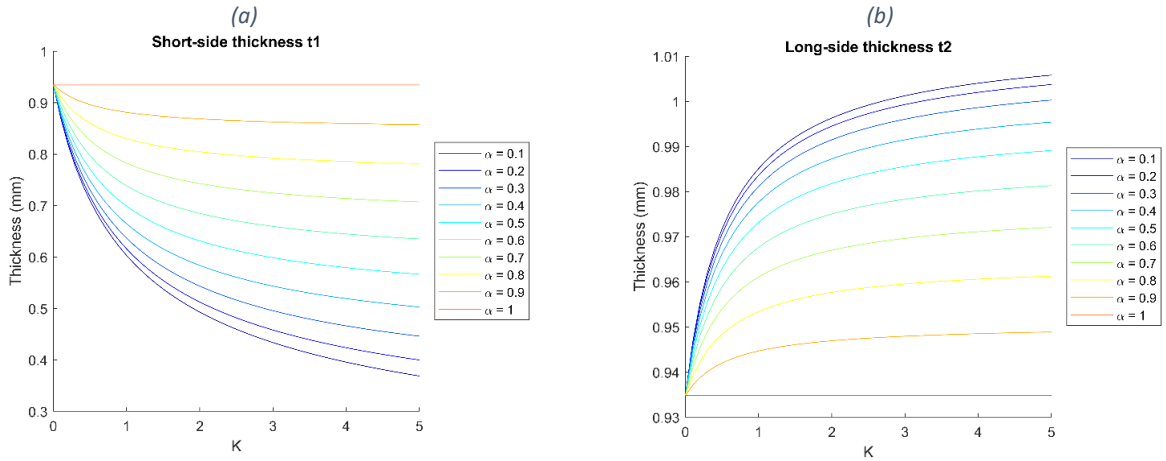

Figure 3: Parametric study on (a) the short-side thickness t_1 and (b) the long-side thickness t_2 as functions of channel aspect ratio ($\alpha = H/h$) and the moment of inertia ratio (K).

A parameter study was performed, given in Fig. 3, to investigate the influence of channel aspect ratio ($\alpha = H/h$) and the moment of inertia ratio (K) on the short-side thickness t_1 (Fig. 3a) and the long-side thickness t_2 (Fig. 3b). Inconel 625 was used for the PCHE channel with an internal pressure of 21.8 MPa and temperature of 1000 K. In Fig. 3a, the channel aspect ratio α varies from square ($\alpha = 1$) to flat ($\alpha = 0.1$), the sensitivity of the short-side thickness (t_1) to the moment of inertia ratio K intensifies. Notably, when $\alpha = 1$, t_1 demonstrates no sensitivity to K. When K is varied from 0 to 5, there is a growing sensitivity of t_1 to alpha with increasing K, except at K = 0 where α sensitivity vanishes. The special case of K = 0 is adopted exclusively in many previous studies [9-12]. Inverse trends are observed for t_1 and t_2 in Fig. 3b.

4. Results and Conclusions

A three-dimensional Pareto surface was produced, given in Figure 4, from a multi-objective optimization using an NSGA-II algorithm for the direct heated – recuperated cycle with the optimization objectives of maximizing cycle efficiency and minimizing individual component mass. The Pareto front in Figure 4 represents a set of optimized objectives, populated within a three-dimensional space. Visualizing trends within this three-dimensional space becomes particularly challenging, especially when dealing with such a high variation of design criteria.

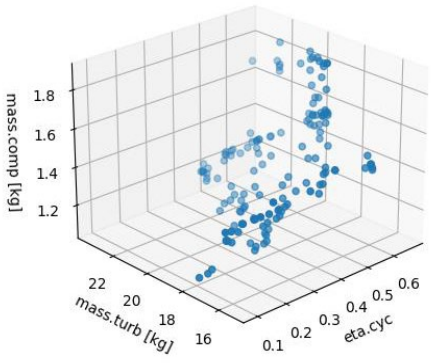

Figure 4: Pareto surface produced from a multi-objective optimization using an NSGA-II algorithm for the direct heated – recuperated cycle

Extraction of "best" solutions from the Pareto front requires further evaluation of the preferred trade-offs within the objective

space and the desired cycle application. Petal plots were produced in Fig. 6 for two representative optimal solutions along the Pareto front and include comparisons of relative magnitudes in optimization objectives and solution variables. In the optimization space, a substantial variation in cycle efficiency values is observed due to the influence of dominant features from both cycle and turbomachinery sizing ML models, respectively. A strong correlation between turbomachinery spindle speed and mass is observed. This overwhelming correlation to RPM caused the component mass in the objective space to be almost entirely dependent on a maximized RPM, with only slight variations due to component efficiency.

This variation caused the most influential variables, as determined by the feature importance metrics of the machine learning model for cycle efficiency (Fig. 8), to stabilize at a similar value throughout the objective space, as shown in Figure 6. This convergence signifies that, once the high-impact variables are optimized, the influence of other variables, typically deemed lower impact, becomes more pronounced in affecting the system's objectives. Essentially, as the critical variables stabilize at optimal values, the contribution of previously minor variables to the objectives becomes more evident. It's important to note that these dynamics were analyzed within a highly variable set of design criteria. When applied to real-world systems, many of these variables will be constrained by specific system requirements, leading to a more focused and precise set of solutions within the objective space.

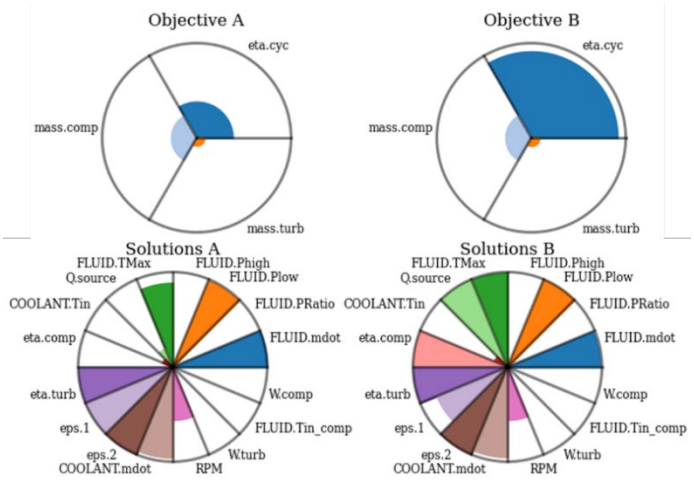

Figure 5: Petal plots for two representative optimal solutions along the Pareto front with comparisons of relative magnitudes in optimization objectives and solution variables.

(a) *(b)*

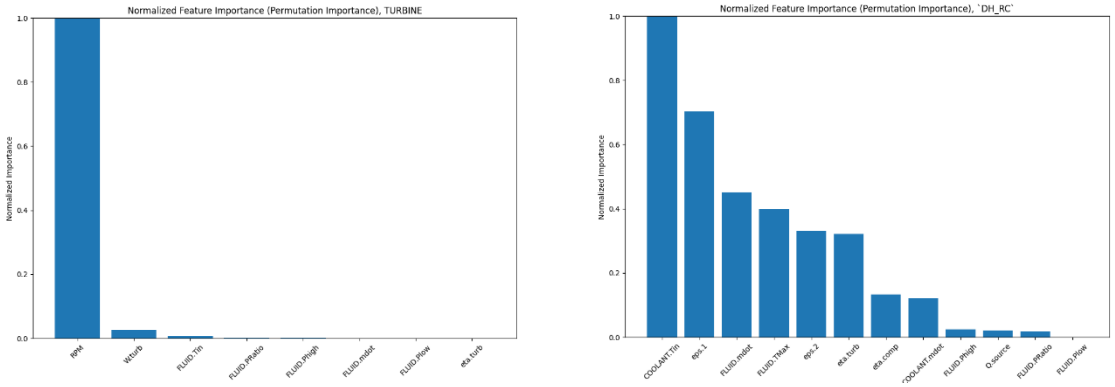

Figure 6: Feature importance plot for (a) trained turbine ML model and (b) trained direct heating – recuperated cycle ML model

The analysis of the PCHEs through the revised stress and sizing criteria has yielded significant insights into the optimization of their design. Namely, there is a widely used specific case (K=0) across past work that should not always be used. The analysis indicated a marked sensitivity of component thickness to both α and K, underscoring the importance of these parameters in the design and optimization of PCHEs. Notably, the analysis revealed a heightened sensitivity of t_1 to K as α shifted from square to flat ratio, and

a heightened sensitivity of t_1 to α as K shifted from 0-5. The same trends are observed with t_2, but with thickness tending to increase with an increase in K and decrease in α.

References

1. Mason LS, Shaltens RK, Dolce JL, Cataldo RL (2002) Status of Brayton cycle power conversion development at NASA GRC. AIP Conference Proceedings 608: 865-871 DOI 10.1063/1.1449813
2. Held TJ, Miller J, Buckmaster DJ A comparative study of heat rejection systems for sCO2 power cycles, pp. 28-31.
3. Angirasa D, Mason LS, Shaltens RK (2003) Radiator Concepts for Nuclear Powered Brayton Conversion Systems. AIP Conference Proceedings 654: 605-612 DOI 10.1063/1.1541345
4. Liang Y, Chen W, Luo X, Chen J, Yang Z, Chen Y (2024) Multi-objective optimization of supercritical CO2 Brayton cycles for coal-fired power generation with two waste heat recovery schemes. Energy Conversion and Management 300: 117962 DOI https://doi.org/10.1016/j.enconman.2023.117962
5. Guo L, Pang L, Zhao J, Yang X (2022) Optimization of Power and Thermal Management System of Hypersonic Vehicle with Finite Heat Sink of Fuel. Energies 15 DOI 10.3390/en15155332
6. Lemmon EW, Bell IH, Huber ML, McLinden MO (2018) NIST standard reference database 23: reference fluid thermodynamic and transport properties-REFPROP, Version 10.0, National Institute of Standards and Technology. Standard Reference Data Program, Gaithersburg
7. Abadi M, Agarwal A, Barham P, Brevdo E, Chen Z, Citro C, Corrado GS, Davis A, Dean J, Devin M (2016) Tensorflow: Large-scale machine learning on heterogeneous distributed systems. arXiv preprint arXiv:160304467
8. Blank J, Deb K (2020) Pymoo: Multi-objective optimization in python. Ieee access 8: 89497-89509
9. Le Pierres R, Southall D, Osborne S Impact of mechanical design issues on printed circuit heat exchangers University of Colorado Bolder.
10. Xu Z, Chen W, Lian J, Yang X, Wang Q, Chen Y, Ma T (2022) Study on mechanical stress of semicircular and rectangular channels in printed circuit heat exchangers. Energy 238: 121655
11. Jiawei W, Yuwei SUN, Mingjian LU, Jian W, Xinping YAN (2023) STRUCTURAL STRESS ANALYSIS OF HYBRID HEAT EXCHANGERS IN THE S-CO 2 POWER CYCLE FOR MARINE WASTE HEAT RECOVERY. Thermal Science 27
12. Nestell J, Sham TL (2015) ASME code considerations for the compact heat exchanger. Oak Ridge National Laboratory, ORNL/TM-2015/401
13. Boiler A (2019) ASME Boiler and Pressure Vessel Code American Society of Mechanical Engineers. Section II, Materials. Part D.
14. Boiler A (2019) ASME Boiler and Pressure Vessel Code American Society of Mechanical Engineers. Section VIII, Rules for Construction of Pressure Vessels. Division 1.